Percolation renormalization-group approach to the q-state Potts model

Chin-Kun Hu
Institute of Physics, Academia Sinica, Nan-Kang, Taipei, Taiwan 115 29, Republic of China

Chi-Ning Chen
Institute of Physics, National Tsing-Hua University, Hsin-Chu, Taiwan 300 43, Republic of China
(Received 9 September 1987; revised manuscript received 19 January 1988)

Based on the connection between the q-state Potts model (QPM) and the q-state bond-correlated percolation model (QBCPM), we have proposed percolation renormalization-group (PRG) methods to calculate the free energy, the critical point, and critical exponents for the QPM. Our methods are free from inconsistency in Larsson's method. We have carried out the $\lambda_1\times\lambda_1$ to $\lambda_2\times\lambda_2$ renormalization-group (RG) transformations in our methods for several values of original cell sizes λ_1 and final cell sizes λ_2 with various boundary conditions. We find that such RG transformations with large λ_1 and λ_2 and periodic boundary condition usually give accurate physical quantities for the QPM. The advantages and generalization of our approach are also discussed.

I. INTRODUCTION

Real-space renormalization-group methods (RSRGM's) have traditionally been applied to Ising-like spin models with spin states as variables and coupling constants as renormalization parameters.[1-3] Such methods have the disadvantage that the number of spin configurations in a unit cell of renormalization-group transformations becomes very large when the number of spin components for each spin is a large number, e.g., the q-state Potts model[4,5] for a large q. In a recent paper Larsson[6] extended a RSRG method for random-percolation problems[7,8] to the q-state bond-correlated percolation model (QBCPM) which has been shown[9-19] or proposed[20(a)] to be the percolation representation of the q-state Potts model.[20(b)] Larsson's method[6] does not have the disadvantage of the traditional RSRGM's mentioned above. However, Larsson's method may not be used to calculate the free energy for the QPM and its formulation also contains some inconsistency which will be discussed below.

In this paper in Sec. II we present two percolation renormalization-group methods for the q-state bond-correlated percolation model (QBCPM)[9-17] corresponding to the q-state Potts model (QPM).[4,5] Our methods may be used to calculate the free energy, the critical point, and critical exponents of the QPM with q as a parameter, but it is free from inconsistency in Larsson's method. In Sec. III we present our calculated phase transition points, critical exponents, and free energies for the square lattice QBCPM and the QPM. In Sec. IV we discuss some advantages and generalizations of our approach.

II. CALCULATION METHODS

Following the derivation of Hu,[10,14,15] we may write the partition function for the QPM on a lattice G of N sites and $\bar{E}$ nearest-neighbor (NN) bonds as follows:

$$\begin{aligned} Z_N &= \sum_{s_1,s_2,\ldots,s_N} \exp\left[K \sum_{\substack{\mathrm{NN}\\ i,j}} \delta(s_i,s_j)\right] \\ &= \sum_{G'\subseteq G} (e^K-1)^{b(G')} q^{n(G')} \\ &= e^{K\bar{E}} \sum_{G'\subseteq G} x^{b(G')} y^{\bar{E}-b(G')} q^{n(G')} , \end{aligned} \tag{1}$$

where $b(G')$ and $n(G')$ are the numbers of occupied bonds and clusters in G', respectively, and

$$x=1-e^{-K},\quad y=1-x=e^{-K} . \tag{2}$$

It should be noted that K is related to the dimensionless Ising coupling constant defined by Onsager[21] as follows:

$$K_I=H=K/2 . \tag{3}$$

It follows from the Euler theorem that

$$n(G')=N-b(G')+N_c(G') , \tag{4}$$

where $N_c(G')$ is the number of closed loops in G'. From (1) and (4), we find that Z_N may also be written as[16]

$$Z_N=q^{N-\bar{E}}(e^K+q-1)^{\bar{E}} \sum_{G'\subseteq G} \bar{x}^{\,b(G')} \bar{y}^{\,\bar{E}-b(G')} q^{N_c(G')} , \tag{5}$$

where

$$\bar{x}=\frac{e^K-1}{e^K+q-1} , \tag{6}$$

$$\bar{y}=1-\bar{x}=\frac{q}{e^K+q-1} . \tag{7}$$

We may use either Eq. (1) or Eq. (5) to formulate RG calculation method, the former will be called "cluster renormalization-group method (CRGM)" [or method 1 (M1)] and the latter will be called "loop renormalization-group method (LRGM)" [or method 2 (M2)]. For each method, we may use either the free boundary condition (FBC), one-sided periodic boundary condition (I-PBC),

and two-sided periodic boundary condition (II-PBC). For the sake of simplicity, in the following we consider RG transformations on a square (SQ) lattice. The extension to other lattices is straightforward.

To construct a RG transformation for the QBCPM on a square lattice, we divide the square lattice of Fig. 1(a) into $\lambda\times\lambda$ cells. A typical $\lambda\times\lambda$ cell is shown in Fig. 1(b). In the free boundary condition (FBC), we generate all possible configurations of b occupied bonds and $E-b$ empty bonds on this cell, and give each configuration a weight according to (1) for the CRGM and (5) for the LRGM. Here $E=2\lambda^2-\lambda$ is the total number of links which connect NN pairs of sites in the cell and the λ sites immediately above the cell. The links for the cell of Fig. 1(b) in the FBC are shown in Fig. 1(c).

In the one-side periodic boundary condition, when we calculate the number of clusters $n(G')$ and the number of loops $N_c(G')$, we assume that the bond configuration for the top row of Fig. 1(c) is the same as the bond configuration for the bottom row of Fig. 1(c).

In the two-sided periodic boundary condition, we generate all possible configurations of b occupied bonds and $E-b$ empty bonds on this cell, and give each configuration a weight according to (1) for the CRGM and (5) for the LRGM. Here $E=2\lambda^2$ is the total number of the links which connect NN pairs of λ^2 sites in the cell, λ sites immediately above the cell, and λ sites immediately at the right-hand side of the cell. The $2\lambda^2$ links for the

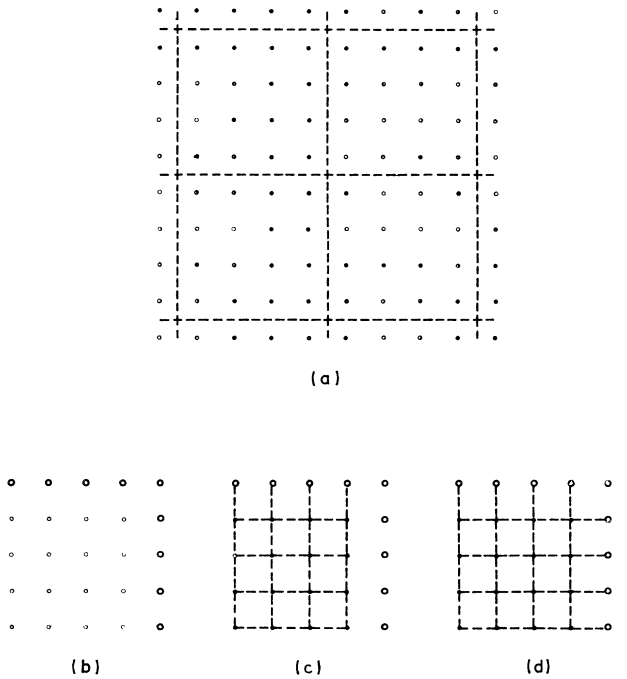

FIG. 1. (a) The square lattice is divided into $\lambda\times\lambda$ cells. In this example $\lambda=4$. (b) A typical $\lambda\times\lambda$ cell. The dots (●) belong to this cell and the open circles (○) belong to adjacent cells. In this example $\lambda=4$. (c) The links on the cell of (b) which are considered to be occupied or unoccupied in the free boundary condition and one-sided periodic boundary condition. The total number of links E is $2\lambda^2-\lambda$. (d) The links on the cell of (b) which are considered to be occupied or unoccupied in the two-sided periodic boundary condition. The total number of links is $2\lambda^2$.

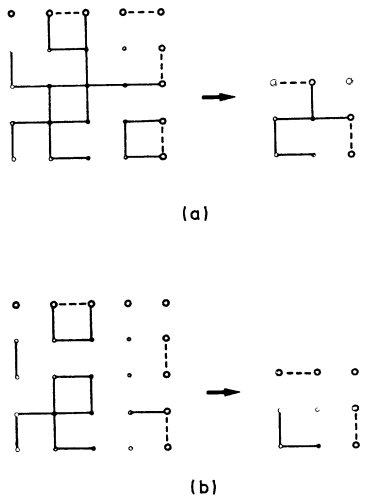

FIG. 2. Renormalization-group transformation from a $\lambda_1\times\lambda_1$ cell to a $\lambda_2\times\lambda_2$ cell. In this example $\lambda_1=4$ and $\lambda_2=2$. (a) From a percolating configuration of a 4×4 cell with two-sided PBC to a percolating configuration of a 2×2 cell with two-sided PBC. The 4×4 configuration gives a contribution to the sum in Eq. (8a) with $b=19$, $n=3$, and $N_c=3$. Note that the dotted "bonds" come from the PBC and two loops come from the additional contribution of dotted bonds. (b) From a nonpercolating configuration of a 4×4 cell with two-sided PBC to a nonpercolating configuration of a 2×2 cell with two-sided PBC. The 4×4 configuration gives a contribution to the sum in Eq. (8b) with $b=13$, $n=7$, $N_c=2$. Note that the dotted "bonds" come from the PBC and one loop comes from the additional contribution of dotted bonds.

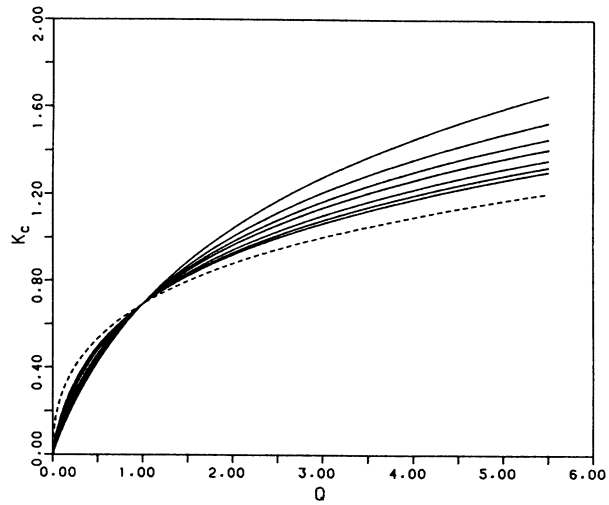

FIG. 3. The fixed points (solid lines) as a function of q obtained from λ_1/λ_2 method 2 RG transformation for various values of λ_1 and λ_2. The dotted line represents the exact solution. Near $q=5$, the curves from up to down positions are obtained, respectively, from $\frac{2}{1}$, $\frac{3}{1}$, $\frac{4}{1}$, $\frac{5}{1}$, $\frac{5}{2}$, $\frac{5}{3}$, and $\frac{5}{4}$ PRG transformations. Note that when λ_1 or λ_2 becomes larger, we have more accurate results.

cell of Fig. 1(b) in the two-sided PBC are shown in Fig. 1(d). When we calculate the number of clusters $n(G')$ and the number of loops $N_c(G')$, we assume that the bond configuration for the top row (the rightmost column) of Fig. 1(d) is the same as the bond configuration for the bottom row (the leftmost column) of Fig. 1(d).

In each of above boundary conditions, we may classify the bond configurations on a cell D into percolating configurations D'_p and nonpercolating configurations D'_f. In the former case, there is a path of occupied bond which connect a site in the lower boundary (bottom row) to a site in the upper boundary (top row). In the later case, there is no such path. Based on such classification, we may define the following partial sums:

$$R(D,x_0,y_0,q_1,q_2)\equiv \sum_{D'_p\subseteq D} x_0^{b(D'_p)} y_0^{E-b(D'_p)} q_1^{n(D'_p)} q_2^{N_c(D'_p)} , \tag{8a}$$

$$Q(D,x_0,y_0,q_1,q_2)\equiv \sum_{D'_f\subseteq D} x_0^{b(D'_f)} y_0^{E-b(D'_f)} q_1^{n(D'_f)} q_2^{N_c(D'_f)} , \tag{8b}$$

where the sum in (8a) is over all D'_p on D and the sum in (8b) is over all D'_f on D; $b(D'_p)$, $n(D'_p)$, and $N_c(D'_p)$ are, respectively, the number of occupied bonds, the number of clusters, and the number of closed loops in D'_p, and similar definitions for $b(D'_f)$, $n(D'_f)$, and $N_c(D'_f)$.

Now consider a $\lambda_1\times\lambda_1$ cell, denoted by D_1, to a $\lambda_2\times\lambda_2$ cell, denoted by D_2, RG transformation shown in Fig. 2, where $\lambda_1>\lambda_2$. Such RG transformation will be denoted as λ_1/λ_2 transformation. We propose that the RG transformation equation may be written as

$$e^{K'_0} R(D_2,x'_0,y'_0,q_1,q_2)=R(D_1,x_0,y_0,q_1,q_2) , \tag{9a}$$

$$e^{K'_0} Q(D_2,x'_0,y'_0,q_1,q_2)=Q(D_1,x_0,y_0,q_1,q_2) , \tag{9b}$$

where K'_0 is a constant which arises from the background energy of the RG transformation and is similar to G in Eq. (1.3) in the book of Burkhardt and Leeuwen.[22] In the CRGM (method 1), we choose

$$q_1=q,\quad q_2=1 , \tag{10}$$

$$x_0=1-e^{-K},\quad y_0=1-x_0=e^{-K} , \tag{11}$$

$$x'_0=1-e^{-K'},\quad y'_0=1-x'_0=e^{-K'} . \tag{12}$$

In the LRGM (method 2), we choose

$$q_1=1,\quad q_2=q , \tag{13}$$

$$x_0=\frac{e^K-1}{e^K+q-1},\quad y_0=1-x_0=\frac{q}{e^K+q-1} , \tag{14}$$

$$x'_0=\frac{e^{K'}-1}{e^{K'}+q-1} , \tag{15}$$

$$y'_0=1-x'_0=\frac{q}{e^{K'}+q-1} . \tag{16}$$

In (12), (15), and (16), K' is the coupling constant for the QPM after the RG transformation.

It should be noted that Eqs. (3.2a) and (3.2b) in Larsson's paper[6] correspond to (9a) and (9b) with $\lambda_2=1$, $K'_0=0$, $q_1=q$, $q_2=1$, $x_0=1-e^{-K}$, $y_0=e^{-K}$ and in the FBC. For $q\neq 1$, usually one cannot find the solution with $x'+y'=1$ from Larsson's RG transformation equations. This is inconsistent with idea that variables before the RG transformation and after the RG transformation should have the same property.[23] By introducing the parameter K'_0, we remove such inconsistency and may find the solution with $x'_0+y'_0=1$. In fact, as we will discuss below we may also calculate the free energy for the QPM from a series of background energies $\{K'_0,K''_0,\ldots\}$ coming from step by step RG transformations. Since in actual calculations, Larsson[6] used the variable $U=x/y$, his calculated fixed point u and critical exponent ν correspond the results of our CRGM with the FBC.

As in the usual real-space RG transformations[1,3,6–8] from the fixed point of (9), x_0^*, we have the phase transition point K_c (being J/k_BT_c) which is related to x_0^* by

$$x_0^*=1-e^{-K_c} \tag{17}$$

in the CRGM and by

$$x_0^*=(e^{K_c}-1)/(e^{K_c}+q-1) , \tag{18}$$

in the LRGM. From the linearized RG transformations near x_0^*, we may calculate the scaling power y_T and the critical exponent ν,

$$\frac{1}{\nu}=y_T=\left[\ln\left[\frac{\partial x'_0}{\partial x_0}\right]\right]_{x_0=x_0^*}\left[\ln\left[\frac{\lambda_1}{\lambda_2}\right]\right]^{-1} . \tag{19}$$

At the fixed point, the average number of total lattice sites in the largest percolating cluster of percolating configurations for the original $\lambda_1\times\lambda_1$ cell and final $\lambda_2\times\lambda_2$ cell of Eq. (9a) are given, respectively, by

$$\langle S(D'_{1p})\rangle=\left[\sum_{D'_{1p}\subseteq D_1} x_0^{b(D'_{1p})} y_0^{E-b(D'_{1p})} q_1^{n(D'_{1p})} q_2^{N_c(D'_{1p})} S(D'_{1p})\right]_{x_0=x_0^*} [R(D_1,x_0^*,y_0^*,q_1,q_2)]^{-1}\propto\lambda_1^D , \tag{20a}$$

$$\langle S(D'_{2p})\rangle=\left[\sum_{D'_{2p}\subseteq D_2} x_0^{b(D'_{2p})} y_0^{E-b(D'_{2p})} q_1^{n(D'_{2p})} q_2^{N_c(D'_{2p})} S(D'_{2p})\right]_{x_0=x_0^*} [R(D_2,x_0^*,y_0^*,q_1,q_2)]^{-1}\propto\lambda_2^D . \tag{20b}$$

Here $S(D'_{1p})$ and $S(D'_{2p})$ are the number of lattice sites in the largest percolating cluster of D'_{1p} and D'_{2p}, respectively, and D is the fractal dimension of the system, which has been shown[6,24] to be the same as the magnetic scaling power y_h. From (20), we may calculate D and y_h from the equation:

$$\left[\frac{\lambda_1}{\lambda_2}\right]^D=\frac{\langle S(D'_{1p})\rangle}{\langle S(D'_{2p})\rangle} . \tag{21}$$

Since

$$R(D_1,x_0^*,y_0^*,q_1,q_2)\neq R(D_2,x_0^*,y_0^*,q_1,q_2) ,$$

Eq. (21) is not the same as Eqs. (3.6) and (3.7) in Larsson's paper[6] even in our CRGM with FBC.

In the CRGM (i.e., M1), the free energy per lattice site may be calculated from (1):

$$-f_1(x,q)=\lim_{N\to\infty}\left[\frac{1}{N}\ln Z_N\right]=\frac{z}{2}K+f_c(x,q) , \tag{22a}$$

where z is the coordination number of the lattice and $f_c(x,q)$ is given by

$$f_c(x,q)=\lim_{N\to\infty}\left[\frac{1}{N}\ln\left[\sum_{G'\subseteq G}x^{b(G')}y^{E-b(G')}q^{n(G')}\right]\right] . \tag{22b}$$

It follows from (9) that $f_c(x',q)$ may be written as

$$f_c(x,q)=\frac{1}{\lambda_1^2}K'_0+\left[\frac{\lambda_2}{\lambda_1}\right]^2 f_c(x',q) , \tag{22c}$$

where $f_c(x',q)$ is the free energy per lattice site calculated from the transformed variable x'. Equation (22c) is similar to Eq. (1.6) in the book of Burkhardt and Leeuwen.[22]

We may iterate (22c) up to the lth RG transformation so that the system approaches the high-temperature fixed point in which $x\to 0$ and each spin has the free energy $\ln q$ or the low-temperature fixed point in which $x\to 1$ and each spin has zero free energy. It follows from (22a) and (22c) that $f_1(x,q)$ may be approximated by

$$-f_1(x,q)=\frac{z}{2}K+\frac{1}{\lambda_2^2}\sum_{a=1}^{l}\left[\frac{\lambda_2}{\lambda_1}\right]^{2a}K_0^{(a)}+\begin{cases}\left[\dfrac{\lambda_2}{\lambda_1}\right]^{2l}\ln q, & \text{for } T>T_c \quad (23a)\\ 0, & \text{for } T<T_c , \quad (23b)\end{cases}$$

where $K_0^{(1)}=K'_0$ and in general $K_0^{(a)}$ is the constant arising from the ath iteration in the CRGM.

In the LRGM (i.e., M2), the free energy per lattice site may be calculated from (5):

$$-f_2(\bar{x},q)=\lim_{N\to\infty}\left[\frac{1}{N}\ln Z_N\right]=\ln q-\frac{z}{2}\ln(1-\bar{x})+f_L(\bar{x},q) , \tag{24a}$$

where

$$f_L(\bar{x},q)=\lim_{N\to\infty}\left[\frac{1}{N}\ln\left[\sum_{G'\subseteq G}\bar{x}^{b(G')}\bar{y}^{E-b(G')}\times q^{N_c(G')}\right]\right] . \tag{24b}$$

Using a procedure similar to that used to derive (23), we find that after a large number (l) of RG transformations $f_2(x,q)$ may be approximated by:

$$-f_2(\bar{x},q)=\ln q-\frac{z}{2}\ln(1-\bar{x})+\frac{1}{\lambda_2^2}\sum_{a=1}^{l}\left[\frac{\lambda_2}{\lambda_1}\right]^{2a}K_0^{(a)}+\begin{cases}\left[\dfrac{\lambda_2}{\lambda_1}\right]^{2l}\ln q, & \text{for } T<T_c \quad (25a)\\ 0, & \text{for } T>T_c , \quad (25b)\end{cases}$$

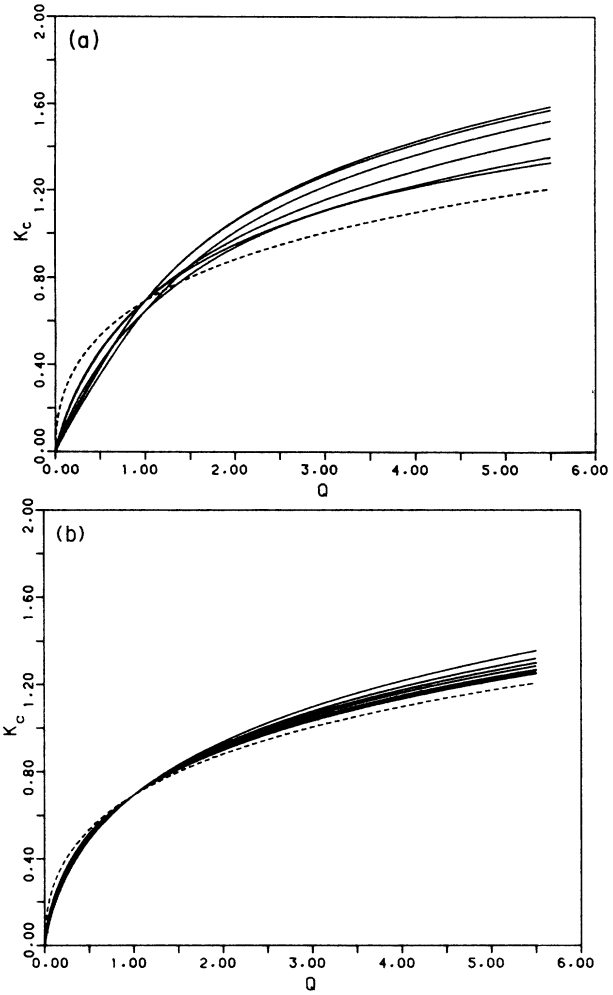

FIG. 4. (a) The fixed points (solid lines) as a function of q obtained from $\frac{3}{2}$ method 1 (M1) and method 2 (M2) RG transformations with various boundary conditions. The dotted line represents the exact solution. Near $q=5$, the curves from up to down positions are obtained, respectively, from $\frac{3}{2}$ (M1), $\frac{3}{2}$ P (M1), $\frac{3}{2}$ PP (M1), $\frac{3}{2}$ (M2), $\frac{3}{2}$ P(M2), and $\frac{3}{2}$ PP (M2) PRG transformations. (b) The fixed points (solid lines) as a function of q obtained from M3 RG transformations. The dotted line represents the exact solution. Near $q=5$, the curves from up to down positions are obtained, respectively, from $\frac{2}{1}$, $\frac{3}{1}$, $\frac{4}{1}$, $\frac{5}{1}$, $\frac{5}{2}$, $\frac{5}{3}$, and $\frac{5}{4}$ PRG transformations.

where $K_0^{(1)}=K_0'$ and in general $K_0^{(a)}$ is the constant arising from the ath iteration in the LRGM.

In method 1 with the free boundary condition, if we consider $n(D_p')$ of (8a) and $n(D_f')$ of (8b) to represent, respectively, the numbers of percolating clusters and nonpercolating clusters in the cell D, which do not connect to sites of the upper cell (e.g., top open sites of Fig. 2), then the RG transformation of (9) will be different from the original transformation. Such new PRG method will be called "reduced cluster renormalization-group method (RCRGM)" or method 3(M3). The calculations of the critical point, the critical exponent, and the free energy in M3 are similar to those in M1. When the idea of M3 is applied to the one-dimensional QPM, the PRG transformation is exact.[25] We expect M3 will give qualitative good results for the square lattice QPM.

Now we discuss how we actually carry out RG transformations of Eq. (9) with computers. The functions $R(D,x_0,y_0,q_1,q_2)$ and $Q(D,x_0,y_0,q_1,q_2)$ of (8) and (9) may be written as

$$R(D,x_0,y_0,q_1,q_2)=\sum_{b=0}^{E}\sum_{n=0}^{\bar{n}} N_p(D,b,n) \times x_0^b y_0^{E-b} q_1^n q_2^{n+b-\bar{n}} , \quad (26a)$$

$$Q(D,x_0,y_0,q_1,q_2)=\sum_{b=0}^{E}\sum_{n=0}^{\bar{n}} N_f(D,b,n) \times x_0^b y_0^{E-b} q_1^n q_2^{n+b-\bar{n}} , \quad (26b)$$

where $\bar{n}$ equals λ^2 and is the total number of sites in the $\lambda\times\lambda$ cell, $N_p(D,b,n)$ and $N_f(D,b,n)$ are, respectively, the total number of the percolating configurations D_p' and the nonpercolating configurations D_f' with b occupied bonds and n clusters. For a large λ, it is very time consuming to calculate $N_p(D,b,n)$ and $N_f(D,b,n)$ directly. To reduce the computing time, we cut a $\lambda\times\lambda$ cell into $\lambda_a\times\lambda$ and $\lambda_b\times\lambda$ cells where $\lambda_a+\lambda_b=\lambda$, and obtain configuration statistical data for such small cells. Using such data, we calculate $N_p(D,b,n)$ and $N_f(D,b,n)$. The detail of such calculation method will be reported elsewhere. Right now, we do not have powerful computing facilities. We use only a PC-AT computer to calculate $N_p(D,b,n)$ and $N_f(D,b,n)$ for λ up to 5. Once we have $N_p(D,b,n)$ and $N_f(D,b,n)$ for λ_1 and λ_2, the calculations of critical points, critical exponents, free energies for various q and K do not need much CPU time. We use a CDC computer to carry out such calculations.

TABLE I. Fixed point for the Ising model K_I calculated by (a) method 1 and (b) method 2 for various boundary conditions and cell sizes. When $\lambda_2=1$ the transformation is called cell to site transformation. Exact $K_I^*=0.44068\ldots$.

Free BC		One-sided Periodic BC		Two-sided Periodic BC	
		(a)			
		Cell to site			
$\frac{2}{1}$	0.6322	$\frac{2}{1}$ P	0.6322	$\frac{2}{1}$ PP	0.5987
$\frac{3}{1}$	0.5769	$\frac{3}{1}$ P	0.5755	$\frac{3}{1}$ PP	0.5462
$\frac{4}{1}$	0.5474	$\frac{4}{1}$ P	0.5455		
$\frac{5}{1}$	0.5288				
		Cell to cell			
$\frac{3}{2}$	0.5298	$\frac{3}{2}$ P	0.5275	$\frac{3}{2}$ PP	0.5026
$\frac{4}{2}$	0.5120	$\frac{4}{2}$ P	0.5093		
$\frac{5}{2}$	0.5003				
$\frac{4}{3}$	0.4949	$\frac{4}{3}$ P	0.4916		
$\frac{5}{3}$	0.4861				
$\frac{5}{4}$	0.4775				
		(b)			
		Cell to site			
$\frac{2}{1}$	0.5216	$\frac{2}{1}$ P	0.4853	$\frac{2}{1}$ PP	0.5113
$\frac{3}{1}$	0.5031	$\frac{3}{1}$ P	0.4797	$\frac{3}{1}$ PP	0.4892
$\frac{4}{1}$	0.4912	$\frac{4}{1}$ P	0.4744		
$\frac{5}{1}$	0.4832				
		Cell to cell			
$\frac{3}{2}$	0.4865	$\frac{3}{2}$ P	0.4744	$\frac{3}{2}$ PP	0.4674
$\frac{4}{2}$	0.4779	$\frac{4}{2}$ P	0.4691		
$\frac{5}{2}$	0.4720				
$\frac{4}{3}$	0.4695	$\frac{4}{3}$ P	0.4639		
$\frac{5}{3}$	0.4650				
$\frac{5}{4}$	0.4606				

TABLE II. Critical exponent ν for the QPM with (a) $q=1$, the conjectured exact value: $\frac{4}{3}=1.333\ldots$; (b) $q=2$, the exact value: 1; (c) $q=3$, the conjectured exact value: $\frac{5}{6}=0.8333\ldots$; (d) $q=4$, the conjectured exact value: $\frac{2}{3}=0.666\ldots$.

Free BC		One-sided periodic BC		Two-sided periodic BC	
		(a)			
		Cell to site			
$\frac{2}{1}$	1.428	$\frac{2}{1}$ P	1.428	$\frac{2}{1}$ PP	1.368
$\frac{3}{1}$	1.380	$\frac{3}{1}$ P	1.380	$\frac{3}{1}$ PP	1.322
$\frac{4}{1}$	1.363	$\frac{4}{1}$ P	1.363		
$\frac{5}{1}$	1.355				
		Cell to cell			
$\frac{3}{2}$	1.305	$\frac{3}{2}$ P	1.305	$\frac{3}{2}$ PP	1.249
$\frac{4}{2}$	1.303	$\frac{4}{2}$ P	1.303		
$\frac{5}{2}$	1.305				
$\frac{4}{3}$	1.301	$\frac{4}{3}$ P	1.301		
$\frac{5}{3}$	1.306				
$\frac{5}{4}$	1.311				
		(b)			
		Method 1			
		Cell to site			
$\frac{2}{1}$	1.251	$\frac{2}{1}$ P	1.213	$\frac{2}{1}$ PP	1.176
$\frac{3}{1}$	1.176	$\frac{3}{1}$ P	1.146	$\frac{3}{1}$ PP	1.103
$\frac{4}{1}$	1.146	$\frac{4}{1}$ P	1.121		
$\frac{5}{1}$	1.130				
		Cell to cell			
$\frac{3}{2}$	1.054	$\frac{3}{2}$ P	1.031	$\frac{3}{2}$ PP	0.9968
$\frac{4}{2}$	1.042	$\frac{4}{2}$ P	1.025		
$\frac{5}{2}$	1.037				
$\frac{4}{3}$	1.023	$\frac{4}{3}$ P	1.012		
$\frac{5}{3}$	1.020				
$\frac{5}{4}$	1.015				
		Method 2			
		Cell to site			
$\frac{2}{1}$	1.312	$\frac{2}{1}$ P	1.173	$\frac{2}{1}$ PP	1.152
$\frac{3}{1}$	1.220	$\frac{3}{1}$ P	1.132	$\frac{3}{1}$ PP	1.134
$\frac{4}{1}$	1.179	$\frac{4}{1}$ P	1.115		
$\frac{5}{1}$	1.157				
		Cell to cell			
$\frac{3}{2}$	1.090	$\frac{3}{2}$ P	1.067	$\frac{3}{2}$ PP	1.106
$\frac{4}{2}$	1.072	$\frac{4}{2}$ P	1.062		
$\frac{5}{2}$	1.062				
$\frac{4}{3}$	1.046	$\frac{4}{3}$ P	1.054		
$\frac{5}{3}$	1.040				
$\frac{5}{4}$	1.033				
		(c)			
		Method 1			
		Cell to site			
$\frac{2}{1}$	1.108	$\frac{2}{1}$ P	1.068	$\frac{2}{1}$ PP	1.042
$\frac{3}{1}$	1.047	$\frac{3}{1}$ P	1.010	$\frac{3}{1}$ PP	0.9691
$\frac{4}{1}$	1.021	$\frac{4}{1}$ P	0.9905		
$\frac{5}{1}$	1.007				

TABLE II. (*Continued*).

Free BC		One-sided periodic BC		Two-sided periodic BC	
			Cell to cell		
$\frac{3}{2}$	0.9015	$\frac{3}{2}$ P	0.8854	$\frac{3}{2}$ PP	0.8547
$\frac{4}{2}$	0.9012	$\frac{4}{2}$ P	0.8832		
$\frac{5}{2}$	0.8973				
$\frac{4}{3}$	0.8799	$\frac{4}{3}$ P	0.8709		
$\frac{5}{3}$	0.8774				
$\frac{5}{4}$	0.8718				
			Method 2		
			Cell to site		
$\frac{2}{1}$	1.241	$\frac{2}{1}$ P	1.041	$\frac{2}{1}$ PP	0.9912
$\frac{3}{1}$	1.131	$\frac{3}{1}$ P	1.002	$\frac{3}{1}$ PP	0.9775
$\frac{4}{1}$	1.082	$\frac{4}{1}$ P	0.9863		
$\frac{5}{1}$	1.055				
			Cell to cell		
$\frac{3}{2}$	0.9811	$\frac{3}{2}$ P	0.9391	$\frac{3}{2}$ PP	0.9647
$\frac{4}{2}$	0.9577	$\frac{4}{2}$ P	0.9340		
$\frac{5}{2}$	0.9451				
$\frac{4}{3}$	0.9248	$\frac{4}{3}$ P	0.9250		
$\frac{5}{3}$	0.9163				
$\frac{5}{4}$	0.9049				
			(d)		
			Method 1		
			Cell to site		
$\frac{2}{1}$	1.016	$\frac{2}{1}$ P	0.9846	$\frac{2}{1}$ PP	0.9638
$\frac{3}{1}$	0.9686	$\frac{3}{1}$ P	0.9319	$\frac{3}{1}$ PP	0.8936
$\frac{4}{1}$	0.9480	$\frac{4}{1}$ P	0.9154		
$\frac{5}{1}$	0.9364				
			Cell to cell		
$\frac{3}{2}$	0.8222	$\frac{3}{2}$ P	0.7977	$\frac{3}{2}$ PP	0.7700
$\frac{4}{2}$	0.8153	$\frac{4}{2}$ P	0.7980		
$\frac{5}{2}$	0.8127				
$\frac{4}{3}$	0.7936	$\frac{4}{3}$ P	0.7856		
$\frac{5}{3}$	0.7915				
$\frac{5}{4}$	0.7852				
			Method 2		
			Cell to site		
$\frac{2}{1}$	1.191	$\frac{2}{1}$ P	0.9582	$\frac{2}{1}$ PP	0.8988
$\frac{3}{1}$	1.072	$\frac{3}{1}$ P	0.9200	$\frac{3}{1}$ PP	0.8811
$\frac{4}{1}$	1.019	$\frac{4}{1}$ P	0.9047		
$\frac{5}{1}$	0.9896				
			Cell to cell		
$\frac{3}{2}$	0.9117	$\frac{3}{2}$ P	0.8579	$\frac{3}{2}$ PP	0.8619
$\frac{4}{2}$	0.8862	$\frac{4}{2}$ P	0.8524		
$\frac{5}{2}$	0.8722				
$\frac{4}{3}$	0.8494	$\frac{4}{3}$ P	0.8422		
$\frac{5}{3}$	0.8396				
$\frac{5}{4}$	0.8260				

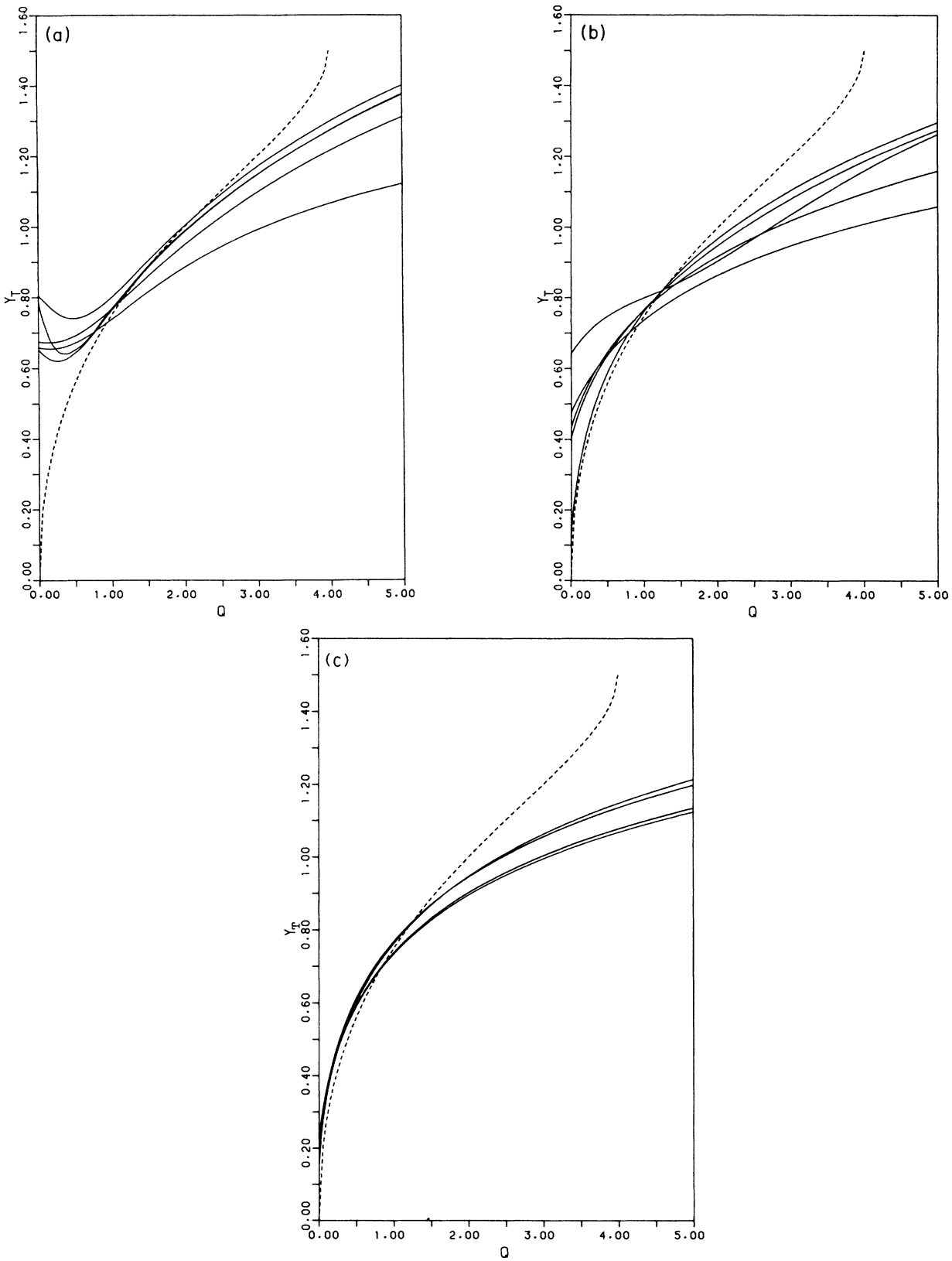

FIG. 5. The thermal scaling power y_T (solid line) as a function of q calculated by (a) method 1, (b) method 2, and (c) method 3. (a) near $q=0$ the curves from up to down positions are obtained, respectively, by $\frac{3}{2}$ PP, $\frac{4}{3}$ P, $\frac{3}{2}$, $\frac{5}{1}$, and $\frac{5}{4}$ PRG transformations. (b) Near $q=0$ the curves from up to down positions are obtained, respectively, by $\frac{3}{2}$ PP, $\frac{5}{1}$, $\frac{3}{2}$, $\frac{4}{3}$ P, and $\frac{5}{4}$ PRG transformations. (c) Near $q=5$ the curves from up to down positions are obtained, respectively, by $\frac{5}{4}$, $\frac{4}{3}$, $\frac{5}{1}$, and $\frac{3}{2}$ PRG transformations. The dotted line represents the conjectured exact solution.

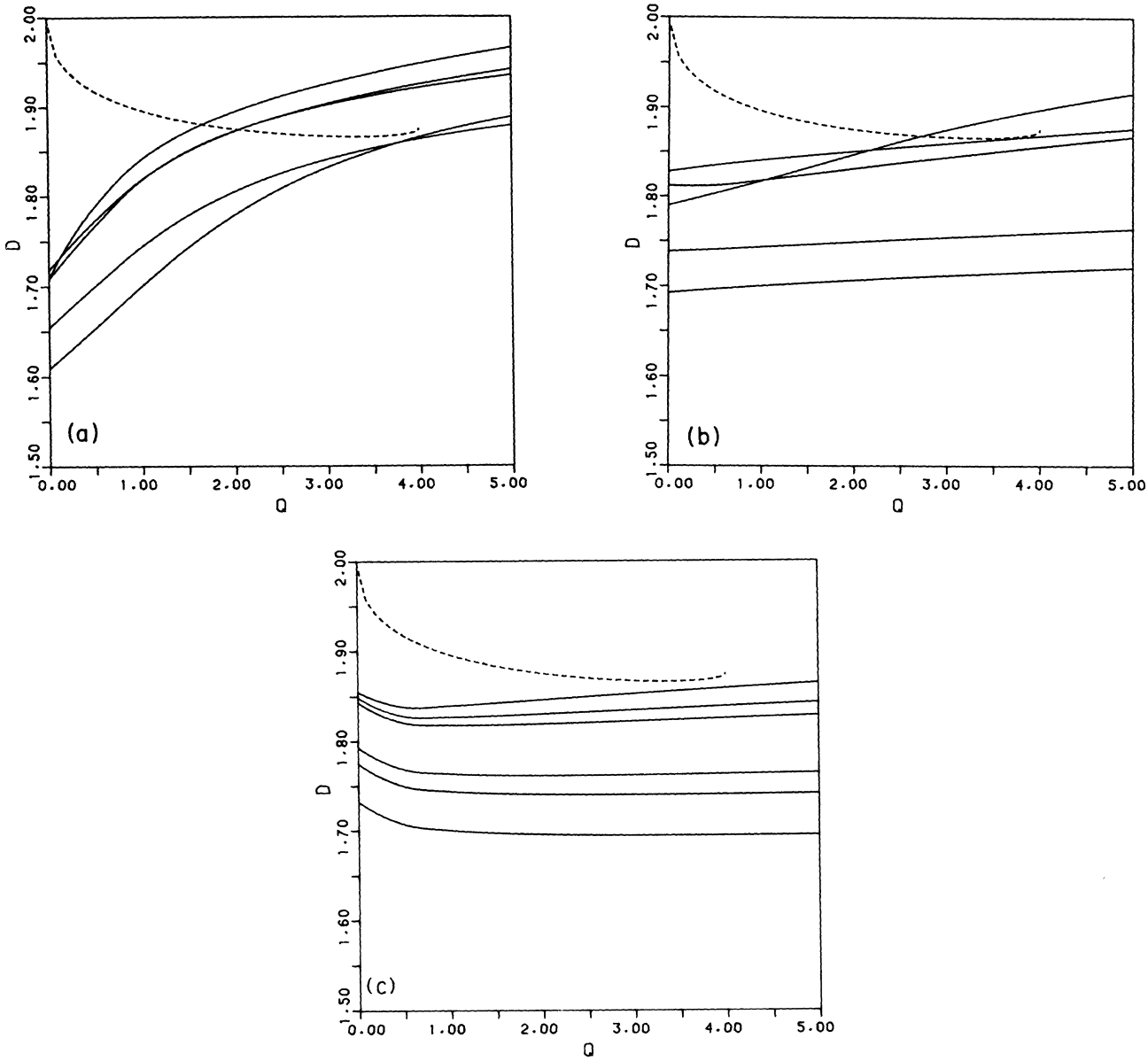

FIG. 6. The fractal dimension D (solid lines) as a function of q calculated by (a) method 1, (b) method 2, and (c) method 3. (a) Near $q=5$ the curves from up to down positions are obtained, respectively, by $\frac{3}{2}$ P, $\frac{3}{2}$, $\frac{3}{2}$ PP, $\frac{2}{1}$, and $\frac{3}{1}$ PRG transformations. (b) Near $q=5$ the curves from up to down positions are obtained, respectively, by $\frac{3}{2}$ PP, $\frac{3}{2}$ P, $\frac{3}{2}$, $\frac{3}{1}$, and $\frac{2}{1}$ PRG transformations. (c) Near $q=0$ the curves from up to down positions are obtained, respectively, by $\frac{4}{3}$, $\frac{4}{2}$, $\frac{3}{2}$, $\frac{4}{1}$, $\frac{3}{1}$, $\frac{3}{1}$, and $\frac{2}{1}$ PRG transformations. The dotted line represents the conjectured exact solution.

III. CALCULATION RESULTS

All results presented in this section are for the square lattice q-state Potts model (QPM), which becomes the simple Ising model[21] when $q=2$. Both cluster renormalization-group methods (method 1 and 3) and loop renormalization-group method (LRGM, method 2) have been used and many original and final-cluster sizes with different boundary conditions (BC) have been considered. Links for the free boundary condition and two-sided periodic boundary condition are shown in Figs. 1(c) and 1(d), respectively, and the former is the same as the case considered by Larsson.[6] In the one-sided periodic boundary condition, only the bonds in the horizontal direction are considered periodic. The $\lambda_1 \times \lambda_1$ cell to $\lambda_2 \times \lambda_2$ cell RG transformations with free BC, one-sided periodic BC, and two-sided periodic BC will be denoted by λ_1/λ_2, $\lambda_1/\lambda_2 P$, and $\lambda_1/\lambda_2 PP$, respectively.

The calculated values of the critical points for the Ising model and the QPM are shown in Table I and Figs. 3 and 4. The calculated values of the critical exponent ν and the thermal scaling power y_T of (19) for the QPM are shown in Table II and Fig. 5. The calculated fractal dimensions for the QPM are shown in Fig. 6. The free en-

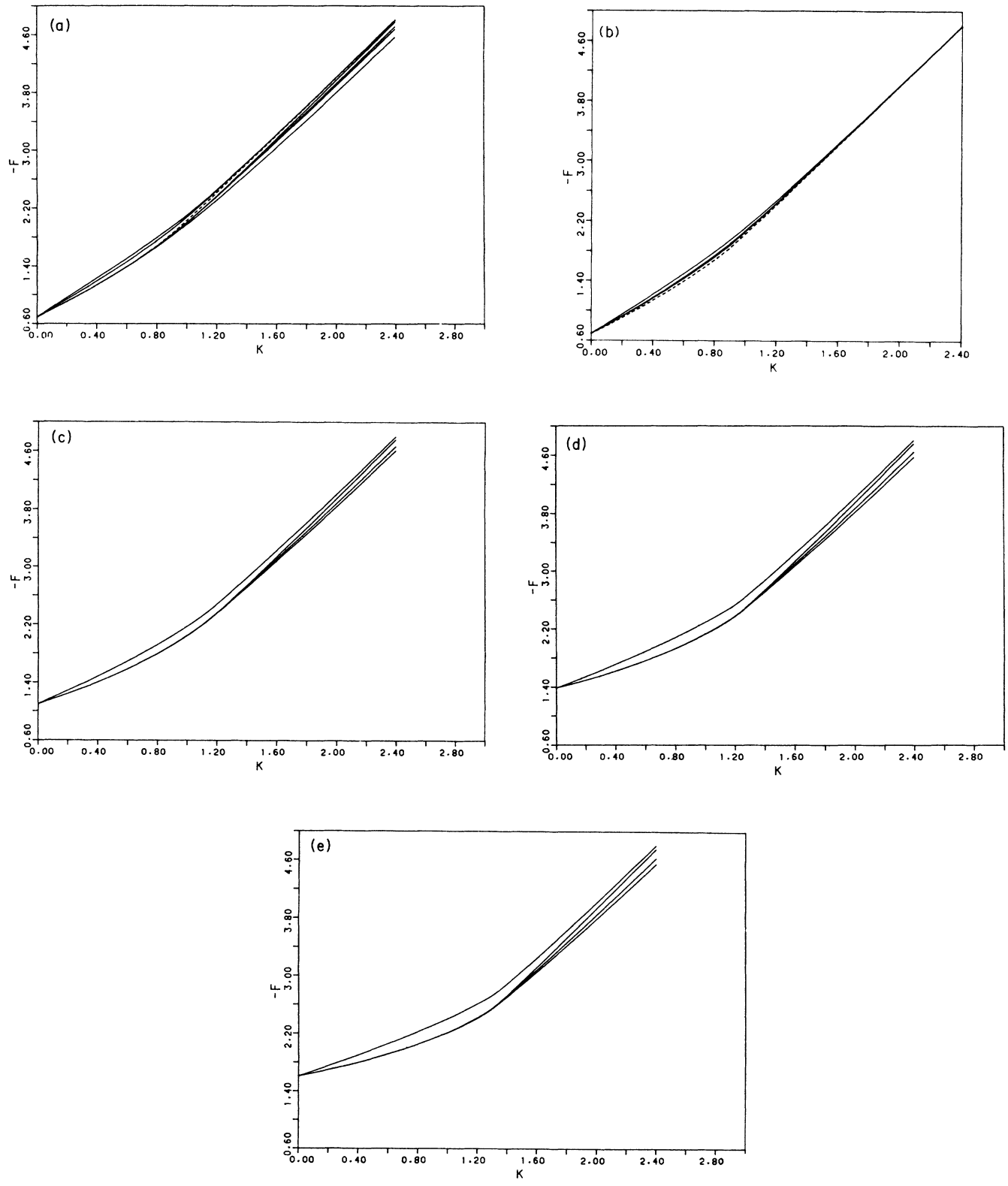

FIG. 7. Free energy (solid lines) of the QPM as a function of K, calculated by method 1 (M1), method 2 (M2), and method 3 (M3) PRG transformations. (a) $q=2$. The dotted line represents the Onsager exact solution. The solid lines from up to down positions are obtained, respectively, by $\frac{3}{2}$ PP (M1), $\frac{5}{4}$ (M1), $\frac{3}{2}$ PP (M2), $\frac{4}{3}$ P (M2), $\frac{5}{4}$ (M2), and $\frac{4}{1}$ (M2) PRG transformations. (b) $q=2$. The dotted line represents the Onsager exact solution. The solid lines from up to down positions are obtained by $\frac{2}{1}$ (M3), $\frac{5}{1}$ (M3), and $\frac{5}{4}$ (M3) PRG transformations. (c) $q=3$. (d) $q=4$. (e) $q=5$. In (c)–(e) the curves from up to down positions are obtained, respectively, by $\frac{5}{4}$ (M1), $\frac{3}{2}$ PP (M2), $\frac{4}{3}$ P (M2), and $\frac{5}{4}$ (M2) PRG transformations.

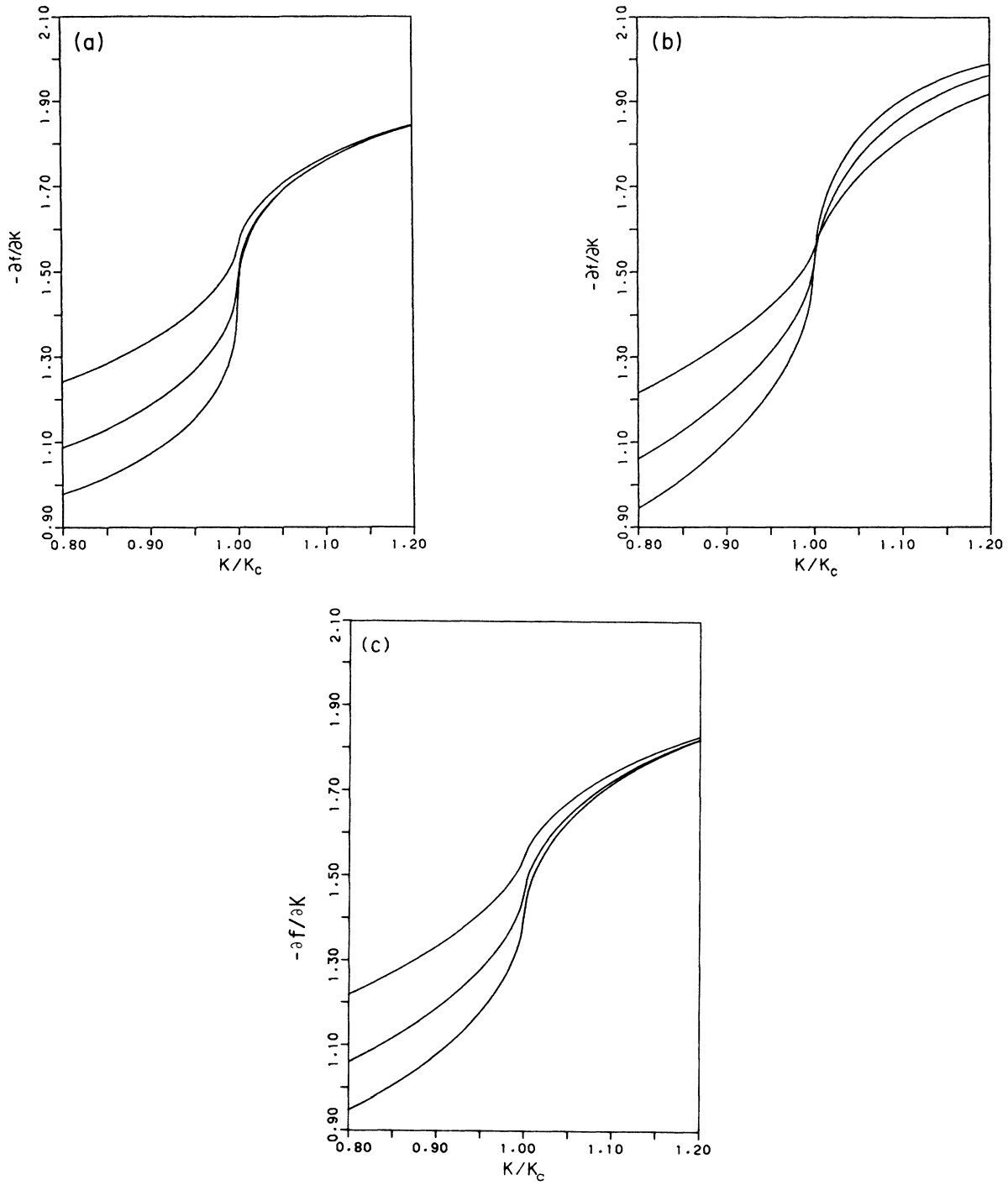

FIG. 8. The first derivative of the free energy for the QPM, $-(\partial f/\partial K)$, as a function of K/Kc obtained by (a) $\frac{5}{4}$ (M1), (b) $\frac{3}{2}$ PP (M2), and (c) $\frac{5}{4}$ (M3) PRG transformations. In all cases near $K/Kc=0.8$, the curves from up to down positions are for $q=3$, 4, and 5, respectively.

ergies and their first and second derivatives for the QPM are shown in Figs. 7–9, respectively.

The above results usually show the following behavior. (1) Accuracy increases with λ_1 and λ_2. (2) Periodic boundary condition improves the accuracy. (3) In the calculation the global property, methods 1 and 3, gives more accurate results in the region $K>K_c$ while method 2 gives more accurate results in the region $K<K_c$ [cf. Figs. 7(a) and 7(b)]. (4) In the calculation of critical exponents, method 2 gives more accurate results in the region $q<1$ and method 1 gives more accurate results in the region $q>1$.

Table II shows that the differences between our best values for ν and the probably exact values of ν are only 1.5% for $q=1$ and $q=2$. For $q=4$ the difference between our best value (0.7700) for ν and the den Nijs[26]

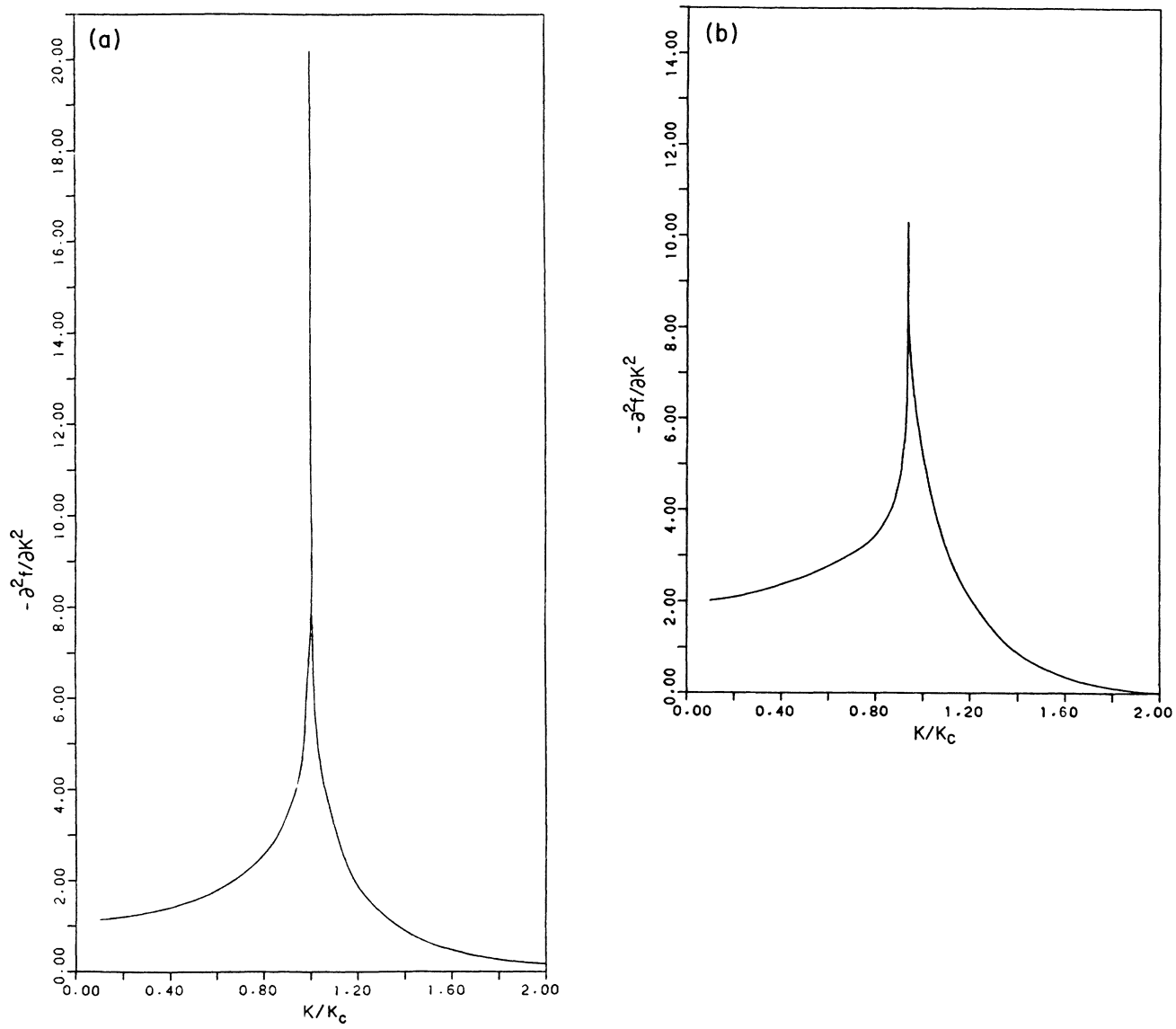

FIG. 9. The second derivative of the free energy for the Ising model, $-(\partial^2 f/\partial K^2)$, as a function of K/Kc obtained by (a) $\frac{5}{3}$ (M1), (b) $\frac{3}{2}$ PP (M2), and (c) $\frac{5}{4}$ (M3) PRG transformations.

conjectured value 0.666... is about 16.5%. Such behavior is similar to Dasgupta's variational RG calculations.[3,5] When Nienhuis, Riedel, and Schick[27] (NRS) enlarged the space of the simple Potts Hamiltonian to that the Potts lattice gas (PLG) and still used the variational RG method, they obtained critical exponent ν very close to den Nijs conjectured value[26] even at $q=4$. We may map the q-state PLG into a q-state site-bond-correlated percolation model[11] (QSBCPM) and extend our method of Sec. II to QSBCPM so that we may calculate the physical quantitied, e.g., ν, for the q-state PLG. It is possible that the accuracy of critical exponents obtained by our methods may be improved by considering PLG as in the work of NRS.[27]

In the limit $q \to 0$, the exact fractal dimension D of the percolating cluster at Tc approaches 2, but our calculations give values smaller than 2. This is due to the fact that in the small cell the number of occupied bonds at Tc, which is $0.5E$ on the average, may not connect all cell sites in the same percolating cluster, therefore D is smaller than the space dimensions. When cell sizes become larger and larger, we expect that the calculated D will approach space dimensions d as $q \to 0$ and the solid curves of Fig. 6 will become closer to the dotted line.[28]

From Fig. 1 it is easy to observe that in the free BC the contributions of closed loops in the boundary between cells are not taken into account and this will cause errors especially in the loop renormalization-group method (LRMG, method 2) in the low-temperature regions. Such observation is confirmed in Fig. 7(a) in which $\frac{3}{2}$ PP results of method 2 are much better than $\frac{4}{3}$ P and $\frac{5}{4}$ results of method 2 in the low-temperature region.

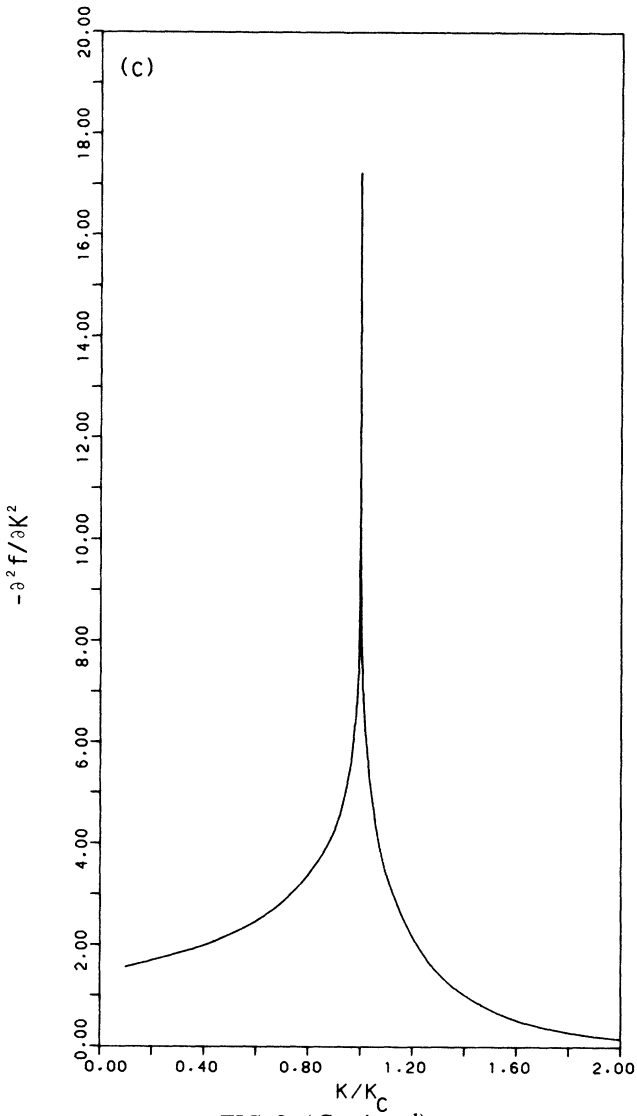

FIG. 9. (*Continued*).

IV. DISCUSSION

There have already been several renormalization-group or finite-size scaling numerical methods which may be used to study the q-state Potts model, e.g., Kadanoff variational method,[29,3] Migdal-Kadanoff method[30] and its modifications,[31] Blöte, Nightingale, and Derrida method,[32,33] Suzuki coherent anomaly method,[34] etc. However, it should be noted that our methods have all of the following advantages.

(1) The number of spin components q enters the calculation scheme as a parameter and may be continued to noninteger values. When q is increased to large numbers, the complexity of calculation does not increase.

(2) In the $\lambda_1 \times \lambda_1$ cell to $\lambda_2 \times \lambda_2$ cell RG transformations, λ_1 and λ_2 may be increased to obtain more accurate results when better computer hardware or languages become available.

(3) The free energy may be calculated from the step by step RG transformations and therefore it may display both the singular behavior near the critical point and the global property of the system from high temperatures to low temperatures. See Figs. 7–9.

Reynolds, Stanley, and Klein[8] have proposed a large cell Monte Carlo method (LCMCM) for random-percolation problems. We may extend this method to the q-state bond-correlated percolation model (QBCPM). However, to simulate equilibrium bond configurations for the QBCPM on an $L \times L$ lattice with traditional method[20(a)] is much more difficult than to simulate bond configurations for the random-bond percolation on the same lattice. To overcome this problem, recently Swendsen and Wang[35] proposed a new Monte Carlo simulation method which violates dynamic universality at second-order phase transition, producing very small values of the dynamic critical exponent. Therefore we may use Swendsen and Wang's method to simulate equilibrium bond configurations and clusters for the QBCPM

on an $L \times L$ lattice and calculate $p^*(L)$ at which incipient percolation clusters appear. We then use the well-known formula $|p^*(L)-p_c|^{-\nu} \sim L$ to find the critical point p_c and exponent ν which is related to scaling power y_T by $y_T = 1/\nu$. From the percolating clusters at $p^*(L)$, we may calculate the fractal dimension D which equals the scaling power[24,6] y_h. Thus the large-cell Monte Carlo renormalization-group (or finite-size scaling) method for the QBCPM is also available.

Using the subgraph expansion method,[36] Hu have obtained percolation or cluster representations of a lattice model of hydrogen bonding,[37] a lattice model of sol-gel phase transition,[38] an Ising model with multispin interactions,[39] and an Ising model with antiferromagnetic interactions,[17] dilute q-state Potts model[11,40] which includes Potts lattice gas[25] and Blume-Emery-Griffiths (BEG) model[41] as special cases, etc. Such percolation or cluster problems may be studied by the percolation renormalization-group methods of Sec. II and the large-cell Monte Carlo renormalization-group (or finite-size scaling) method discussed in the previous paragraph.

ACKNOWLEDGMENTS

The author thanks Professor D. Kim, Professor M. Aizenman, Professor R. B. Griffiths, Professor R. H. Swendsen, and Professor M. Kaufman for drawing his attention the works of Kelland, Refs. 19 and 35, and the work of Kaufman and Andelman. The work was supported by the National Science Council of the Republic of China under Contract No. NSC77-0208-M001-35. One of the authors (C.-N.C.) began to do this research at the Institute of Physics, National Taiwan University.

[1]S.-K. Ma, *Modern Theory of Critical Phenomena* (Benjamin, New York, 1976).

[2]*Real-Space Renormalization,* edited by T. W. Burkhardt and J. M. J. van Leeuwen (Springer-Verlag, Berlin, 1982).

[3]C. Dasgupta, Phys. Rev. B **14**, 1221 (1976); **15**, 3460 (1977).

[4]R. B. Potts, Proc. Cambridge Philos. Soc. **48**, 106 (1952).

[5]F. Y. Wu, Rev. Mod. Phys. **54**, 235 (1982).

[6]T. A. Larsson, J. Phys. A **19**, 2383 (1986).

[7]P. J. Reynolds, W. Klein, and H. E. Stanley, J. Phys. C **10**, L167 (1977).

[8]P. J. Reynolds, H. E. Stanley, and W. Klein, J. Phys. A **11**, L199 (1978); Phys. Rev. B **21**, 1223 (1980).

[9]C.-K. Hu, Physica **119A**, 609 (1983).

[10]C.-K. Hu, Phys. Rev. B **29**, 5103 (1984).

[11]C.-K. Hu, Phys. Rev. B **29**, 5109 (1984).

[12]C.-K. Hu, Chin. J. Phys. (Taipei) 22(1), 1 (1984); 22(4), 1 (1984).

[13]C.-K. Hu, Phys. Rev. B **32**, 7325 (1985).

[14]C.-K. Hu, J. Phys. A **19**, 3067 (1986).

[15]C.-K. Hu, Phys. Rev. B **34**, 6280 (1986).

[16]C.-K. Hu, Annu. Rep. Inst. Phys. Acad. Sin. (Taipei) **16**, 105 (1986); J. Phys. A **20**, 6617 (1987).

[17]C.-K. Hu, in *Proceedings of the 1986 Summer School on Statistical Mechanics, Taipei,* edited by C.-K. Hu (Institute of Physics, Academia Sinica and Physics Society of the Republic of China, Taipei, 1987), pp. 91–117.

[18]C.-K. Hu, The History of Science Newsletter (Taipei) Suppl. **5**, 80 (1986) (in Chinese). This paper gives a historical review of this and related developments.

[19]M. Kaufman and D. Andelman, Phys. Rev. B **29**, 4010 (1984).

[20](a) M. Sweeny, Phys. Rev. B **27**, 4445 (1983); (b) see also, A. Coniglio and W. Klein, J. Phys. A **13**, 2775 (1980); A. Coniglio, F. di Liberto, and G. Monroy, *ibid.* **14**, 3017 (1981); G. F. Tuthill and W. Klein, *ibid.* **15**, L377 (1982); A. Coniglio and F. Peruggi, *ibid.* **15**, 1873 (1982); Ref. 6 of the present paper.

[21]L. Onsager, Phys. Rev. **65**, 117 (1944). Onsager used the notation H for the Ising dimensionless coupling constant but in our paper we use the notation K_I.

[22]See *Real-Space Renormalization,* Ref. 2, p. 4.

[23]Equation (2.11) of Ref. 6 is also incorrect.

[24]H. E. Stanley, J. Phys. A **10**, L211 (1977); S. Kirkpatrick, in *Electrical Transport and Optical Properties of Inhomogeneous Media* (Ohio State University, 1977), Proceedings of the First Conference on the Electrical Transport and Optical Properties of Inhomogeneous Media, AIP Conf. Proc. No. 40, edited by J. C. Garland and D. B. Tanner (AIP, New York, 1978), p. 99.

[25]C.-K. Hu and C.-N. Chen (unpublished).

[26]M. P. M. den Nijs, J. Phys. A **12**, 1857 (1979).

[27]B. Nienhuis, E. K. Riedel, and M. Schick, Phys. Rev. Lett. **43**, 737 (1979); J. Phys. A **13**, L31 (1980).

[28]For a discussion of the effect of cluster sizes on the accuracy of critical exponents, see also M. Kaufman and K. K. Mon, Phys. Rev. B **29**, 1451 (1984).

[29]L. P. Kadanoff, A. Houghton, and M. C. Yalabik, J. Stat. Phys. **14**, 171 (1976).

[30]A. A. Migdal, Zh. Eksp. Teor. Fiz. **69**, 810 (1975) [Sov. Phys.—JETP **42**, 413 (1975)]; **69**, 1457 (1975) [**42**, 743 (1975)]; L. P. Kadanoff, Ann. Phys. (NY) **100**, 359 (1976).

[31]J. S. Walker, Phys. Rev. B **26**, 3792 (1982); H. H. Chen, Felix Lee, and H. C. Tseng, Phys. Rev. **34**, 6448 (1986).

[32]H. W. J. Blöte, M. P. Nightingale, and B. Derrida, J. Phys. A **14**, L45 (1981).

[33]H. W. J. Blöte and M. P. Nightingale, Physica **116A**, 405 (1982).

[34]M. Suzuki and M. Katori, J. Phys. Soc. Jpn. **55**, 1 (1986); M. Suzuki, *ibid.* **55**, 4205 (1986).

[35]R. H. Swendsen and J.-S. Wang, Phys. Rev. Lett. **58**, 86 (1987).

[36]The method has been applied to a zero-field QPM or a QPM with the external field coupled with one component of the Potts spins by R. J. Baxter [J. Phys. C **6**, L445 (1973)]; S. B. Kelland [Ph.D. thesis, 1976 (unpublished)], and F. Y. Wu [J. Stat. Phys. **18**, 115 (1978)].

[37]C.-K. Hu, J. Phys. A **16**, L321 (1983).

[38]C.-K. Hu, Annu. Rep. Inst. Phys. Acad. Sin. (Taipei) **14**, 7 (1984).

[39]C.-K. Hu, Chin. J. Phys. (Taipei) **23**, 47 (1985).

[40]C.-K. Hu (unpublished).

[41]M. Blume, V. J. Emery, and R. B. Griffiths, Phys. Rev. A **4**, 1071 (1971).